Similarity Scales and Universal Profiles of Statistical Moments in the Convective Boundary Layer

ZBIGNIEW SORBJAN

CIMMS, The University of Oklahoma, Norman, Oklahoma

(Manuscript received 7 June 1988, in final form 15 February 1990)

ABSTRACT

The parameterization of the mixed layer based on a decomposition of statistical moments into nonpenetrative and residual components and on their local similarity is discussed. The method is examined by using laboratory data for nonpenetrative convection and large-eddy simulation (LES) results for penetration convention. The examination allows discussion of various scales and similarity functions in the convective atmospheric boundary layer. Local similarity is demonstrated to be equivalent to a Level-2 closure scheme of Mellor and Yamada. The derived similarity functions are shown to agree with experimental data and with the results of numerical simulation.

1. Introduction

Deardorff (1970) proposed that turbulent quantities in the bulk of the horizontally homogeneous mixed layer are universal functions of dimensionless height z/z_i, when scaled by the following mixed layer scales:

$$\begin{aligned} w_* &= (\beta z_i Q_0)^{1/3} && \text{(for velocity)} \\ \Theta_* &= Q_0/w_* && \text{(for temperature)} \\ q_* &= M_0/w_* && \text{(for humidity)} \\ z_i & && \text{(for height)} \end{aligned} \tag{1}$$

where Q_0 is the surface potential temperature flux, M_0 is the surface moisture (or other passive scalar) flux, $\beta = g/\Theta_0$ is the buoyancy parameter, and z_i is the height of the mixed layer (all symbols are listed in the Appendix). The mixed layer scaling (1) was found to be valid in both the natural and simulated convective boundary layers. As a result, since the early seventies, measurements in the mixed layer have been traditionally expressed in terms of the mixed layer scales. However, no theoretical predictions regarding the form of the universal functions in the mixed layer have been provided.

In the surface layer a general form of such functions was predicted by the Monin–Obukhov similarity theory for neutral, extremely stable, and convective conditions. In the convective case, surface layer similarity functions were usually formulated in terms of local (z-dependent), free-convection scales, defined as (Wyngaard et al. 1971):

$$\begin{aligned} u_f &= (\beta z Q_0)^{1/3} && \text{(for velocity)} \\ \theta_f &= Q_0/u_f && \text{(for temperature)} \\ q_f &= M_0/u_f && \text{(for humidity)} \\ z & && \text{(for height).} \end{aligned} \tag{2}$$

The local free-convection scaling enabled similarity functions to be expressed in a concise form. For instance, for the temperature and humidity variance it was obtained:

$$\begin{aligned} \overline{\theta'^2}/\theta_f^2 &= C_{\theta b} \\ \overline{q'^2}/q_f^2 &= C_{qb} \end{aligned} \tag{3}$$

where $C_{\theta b}$ and C_{qb} are universal constants.

Similarity predictions were empirically proven to be valid for statistical moments of vertical velocity, temperature, and humidity in the free-convection surface layer; however, their simple extension above this layer was unsuccessful. During the last 20 years, the lack of a theoretical formulation for scaled quantities in the mixed layer resulted in a variety of empirical "best-fit" profiles. In agreement with the observations, all empirical curves followed the free convection predictions in the lower portion of the mixed layer. In its upper portion, a substantial scatter was reported mostly as a result of entrainment from the upper inversion layer. This scatter suggested the list of parameters provided by Deardorff was not complete.

There have been attempts in the past to modify (1) in a way to include the effects of entrainment. For instance, Guillement et al. (1983) expressed statistical

Corresponding author address: Zbigniew Sorbjan, CIMMS, The University of Oklahoma, Norman, OK 73019.

moments of temperature and humidity in the mixed layer in terms of new scales Q_{**}, q_{**}. The new scales were based on the mixed layer scales (1) and in addition on temperature and humidity lapse rates Γ, Γ_q in the upper inversion layer. Moeng and Wyngaard (1984) employed the set of mixed layer scales, extended by two new parameters: the flux ratios $R = Q_i/Q_0$, for the temperature field and $R_q = M_i/M_0$, for the humidity field, where subscripts 0 and i indicate values of the fluxes at the surface and at the top of the mixed layer. Sorbjan (1988, 1989) employed the parameter R for temperature fields, both parameters R and R_q for humidity fields, and also the parameter $D = \Delta/zi$, where Δ is the depth of the interfacial layer on the top of the mixed layer (in Fig. 1, $\Delta = h_2 - z_i$).

The form of the similarity functions describing a vertical distribution of means, variances and convariances of the potential temperature and concentration of a passive scalar were derived by Moeng and Wyngaard (1984) who used the "bottom-up and top-down" decomposition and employed results of a large-eddy simulation (LES) model. Sorbjan (1988, 1989) obtained similarity functions for certain statistical moments of the vertical wind velocity, potential temperature and concentration of a passive scalar in the mixed layer by using arguments of dimensional analysis.

Results obtained by Sorbjan (1988) were based on two hypotheses. According to the first one, a statistical moment X involving vertical velocity, temperature, and/or concentration of a passive species can be decomposed into two components, the nonpenetrative and the residual:

$$X = X_b + X_t \tag{4}$$

where index "b" in the above equation refers to a nonpenetrative component and index "t" refers to a residual (penetrative minus nonpenetrative) component. The physical meaning of the b-term in (4) is associated with nonpenetrative convection, when the heat flux on the top of the mixed layer is zero. Nonpenetrative convection was simulated in a tank by Adrian et al. (1986). In the atmosphere, it can occur during the day when there is no penetration of the inversion layer by thermals. The second term in (4) is zero during nonpenetrative convection and nonzero during penetrative convection.

As shown experimentally by Adrian et al. (1986), statistical moments in nonpenetrative convection have values very close to those during penetrative convection, except in the upper part of the convective boundary layer. This fact explains a physical sense of the decomposition (4): a statistical moment is split into a part that would be generated during nonpenetrative convection and on the "corrective" term including the effects of entrainment.

According to the second hypothesis, each of the components in (4) can be scaled by two sets of local (z-dependent) scales U_b, Θ_b, q_b, z and U_t, Θ_t, q_b, Z, the first for b-components in (4):

$$\begin{aligned} U_b &= [\beta z \overline{w'\theta'_b}(z)]^{1/3} && \text{(for velocity)} \\ \Theta_b &= \frac{\overline{w'\theta'_b}(z)}{U_b} && \text{(for temperature)} \\ q_b &= \frac{\overline{w'q'_b}(z)}{U_b} && \text{(for humidity)} \\ z & && \text{(for height)} \end{aligned} \tag{5}$$

and the second for t-components:

$$\begin{aligned} U_t &= [\beta(z_i + \Delta - z)\overline{w'\theta'_t}(z)]^{1/3} && \text{(for velocity)} \\ \Theta_t &= \frac{\overline{w'\theta'_t}(z)}{U_t} && \text{(for temperature)} \\ q_t &= \frac{\overline{w'q'_t}(z)}{U_t} && \text{(for humidity)} \\ Z &= z_i + \Delta - z && \text{(for height)} \end{aligned} \tag{6}$$

where $\overline{w'\theta'_b}$, $\overline{w'\theta'_t}$, $\overline{w'q'_b}$ and $\overline{w'q'_t}$ are the b- and t-components of temperature and moisture (passive scalar) fluxes defined by (4). It can be noted that the t-scales in (6) are finite and nonzero on the top of the mixed layer if $\Delta \neq 0$.

Scales (5) were obtained by substituting the local value of the b-component of the temperature flux for the surface value in (2). Scales (6) were obtained analogously by substituting the local value of the t-component of the temperature flux in (2) for the surface value and by hypothesizing that the distance from the upper inversion layer $Z = z_i + \Delta - z$ is the height scale. This choice of the length scale is analogous to that of Prandtl who assumed proportionality between the mixing length and the wall distance.

According to the parameterization proposed by Sorbjan (1988), the b-components of certain statistical moments are constant when scaled by the b-scales in (5) while the certain t-components are constant when scaled by the t-scales in (6):

$$\begin{aligned} \frac{X_b}{U_b^a \Theta_b^b q_b^c z^d} &= \text{const} \\ \frac{X_t}{U_t^a \Theta_t^b q_t^c Z^d} &= \text{const} \end{aligned} \tag{7}$$

where a, b, c, and d are constant power coefficients depending on the dimension of the quantity X.

It should be noted that the "local similarity" in the mixed layer is based on the similarity of decomposed profiles of various characteristics of turbulence in the mixed layer. The term "local" applies only to the vertical direction and explains that the adopted scales are dependent on the actual distances from the top and the bottom of the mixed layer. The physical sense of

"local similarity" in the mixed layer is, therefore, different from the case of "local similarity" in the stable boundary layer (Sorbjan 1986), which has a z-independent structure.

In this paper, hypotheses (7) are discussed and compared with empirical data and LES model results. Section 2 considers the nonpenetrative convection and section 3 discusses the penetrative case.

2. Nonpenetrative regime

a. Governing equations

Let us first consider an extreme case of the convective boundary layer in which the production of turbulent kinetic energy is solely due to buoyancy. The mean wind shear is assumed to be negligible causing the flux Richardson number to be large:

$$R_f = \beta\overline{w'\theta'}/[\overline{u'w'}\partial U/\partial z + \overline{v'w'}\partial V/\partial z] \to -\infty. \quad (8)$$

During nonpenetrative convection, rising fluid is initially accelerated by buoyancy. The acceleration decreases with height because thermals lose their buoyancy through a heat transfer to the surrounding fluid. Deceleration occurs when updrafts encounter a descending flow or when they approach the upper boundary. At the top of the boundary layer a slight compression forces the fluid not to accumulate. In this way, the downward motion an be initiated for some of the active fluid, even in the absence of significant negative buoyancy. The rest of the active air spreads horizontally, exchanging vertical kinetic energy for horizontal kinetic energy. After this horizontal spreading, the temperature of air that was formerly in thermals becomes lower than the mean temperature of the mixed layer, which is steadily warming. Consequently, the ascending thermals are converted into a cool, descending flow. Descending fluid is slow because its negative buoyancy is small, and as a result of mass conservation, it occupies a larger area than the faster rising updrafts.

The mean temperature as well as humidity fields in the considered case are assumed to be horizontally homogeneous and obey the following equations:

$$\frac{\partial\Theta}{\partial t} = -\frac{\partial\overline{w'\theta'}}{\partial z}$$

$$\frac{\partial q}{\partial t} = -\frac{\partial\overline{w'q'}}{\partial z} \quad (9)$$

where the radiative flux divergence is neglected in the first equation.

Laboratory experiments (Willis and Deardorff 1974) show that in the early stage of convection, the entire mixed layer warms up ($\partial\Theta/\partial t > 0$, for $0 < z < z_i$) and increases its depth ($\partial z_i/\partial t \geq 0$). Above the mixed layer, in the stable air layer, the temperature does not change with time ($\partial\Theta/\partial t = 0$, for $z \geq z_i$). Taking this into consideration and integrating (9a), it can be obtained that for $z \geq z_i$:

$$\overline{w'\theta'}(z) = \int_z^\infty \frac{\partial\Theta}{\partial t}\, dz = 0. \quad (10)$$

This indicates that the turbulent heat flux is zero at the top of the mixed layer and above this level.

In the later stage of convection, the top of the mixed layer cools down ($\partial\Theta/\partial t < 0$, for $z_i < z < h_2$). This cooling indicates the presence of penetrative convection and the appearance of a negative heat flux:

$$\overline{w'\theta'}(z) = \int_z^{h_2} \frac{\partial\Theta}{\partial t}\, dz < 0 \quad (11)$$

in the layer $h_1 < z < h_2$, where h_1 and h_2 are the levels at which the heat flux is zero (Fig. 1). Penetrative convection case is discussed in section 3.

Equation (9) can be closed by using the Level-2 closure scheme derived by Mellor and Yamada (1974) and Yamada and Mellor (1975). The closing equations for $\overline{w'q'}$, $\overline{w'q'}$, $\overline{\theta'q'}$, $\overline{\theta'^2}$, $\overline{q'^2}$, e^2 and $\overline{w'^2}$ respectively, in the stress-free case have the following form:

$$\overline{w'\theta'} = -3\frac{l_2}{e}\left[\overline{w'^2}\frac{\partial\Theta}{\partial z} - \beta\overline{\theta'^2}\right]$$

$$\overline{w'q'} = -3\frac{l_2}{e}\left[\overline{w'^2}\frac{\partial q}{\partial z} - \beta\overline{\theta'q'}\right]$$

$$\overline{\theta'q'} = -\frac{L}{2e}\left[\overline{w'\theta'}\frac{\partial q}{\partial z} + \overline{w'q'}\frac{\partial\Theta}{\partial z}\right]$$

$$e\frac{\overline{\theta'^2}}{\Lambda_2} = -\overline{w'\theta'}\frac{\partial\Theta}{\partial z}$$

$$e\frac{\overline{q'^2}}{\Lambda_2} = -\overline{w'q'}\frac{\partial q}{\partial z}$$

$$e^3 = \Lambda_1\beta\overline{w'\theta'}$$

$$\overline{w'^2} = \frac{e^2}{3} + \frac{l_1}{e}4\beta\overline{w'\theta'} \quad (12)$$

where $e^2 = \overline{u'^2} + \overline{v'^2} + \overline{w'^2}$ (twice the turbulent kinetic energy), and l_1, l_2, L, Λ_1 and Λ_2 are mixing lengths.

The above second moment equations give a poor approximation of the turbulence in the case of penetrative convection. The reason is the degeneration of the system at the level $z = h_1$ (Fig. 1), where the turbulent heat flux is zero. In this case, the turbulent kinetic energy as well as other moments of temperature vanish. System (12) is free of this flaw in the nonpenetrative case. Taking this case into consideration and assuming that all the mixing lengths are proportional to height, after some algebraic manipulations, it can be shown that each statistical moment in (12) can be expressed in terms of β, $\overline{w'\theta'}$, $\overline{w'q'}$ and z. Using (5), this result can be rewritten in the form:

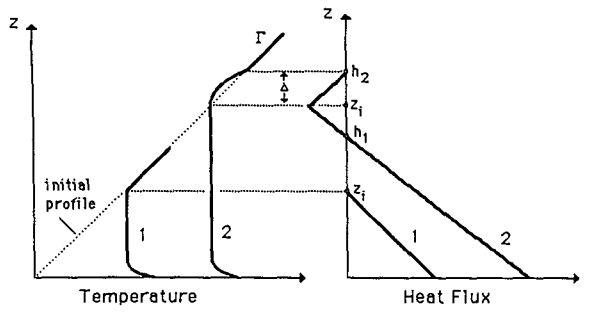

FIG. 1. A vertical structure of the mixed layer during 1) non-penetrative convection, and 2) penetrative convection.

$$\frac{\overline{w_b'^2}}{U_b^2} = \text{const}$$

$$\frac{\overline{\theta_b'^2}}{\Theta_b^2} = \text{const}$$

$$\frac{\overline{q_b'^2}}{q_b^2} = \text{const}$$

$$\frac{\overline{\theta' q_b'}}{\Theta_b q_b} = \text{const}$$

$$\frac{z}{\Theta_b}\frac{\partial \Theta_b}{\partial z} = \text{const}$$

$$\frac{z}{q_b}\frac{\partial q_b}{\partial z} = \text{const} \qquad (13)$$

where subscript b indicates that the moment applies only to the nonpenetrative case.

The obtained equations extend the local free-convection similarity expressed by (3) for the entire nonpenetrative convection mixed layer. They are consistent with the similarity prediction (7a). Consequently, local similarity in the nonpenetrative mixed layer is equivalent to the Level-2 closure model, according to Mellor and Yamada's (1974) hierarchy.

The obtained local similarity can be generalized to derive profiles of other statistical moments. For instance, it can be hypothesized that

$$\frac{\overline{\theta'^2 w_b'}}{\Theta_b^2 U_b} = \text{const}$$

$$\frac{\overline{w'^2 \theta_b'}}{U_b^2 \Theta_b} = \text{const}$$

$$\frac{\overline{w_b'^3}}{U_b^3} = c_{3b}. \qquad (14)$$

Using (5) and taking into consideration the usually observed linearity of the turbulent fluxes with height:

$$\overline{w'\theta_b'}(z) = Q_0(1 - z/z_i)$$

$$\overline{w'q_b'}(z) = M_0(1 - z/z_i) \qquad (15)$$

the explicit form of local scales can be derived:

$$U_b = w_*(z/z_i)^{1/3}(1 - z/z_i)^{1/3}$$

$$\Theta_b = \Theta_* \frac{(1 - z/z_i)^{2/3}}{(z/z_i)^{1/3}}$$

$$q_b = q_* \frac{(1 - z/z_i)^{2/3}}{(z/z_i)^{1/3}}. \qquad (16)$$

From (13), (14) and (16), it can be obtained that

$$\frac{\sigma_{wb}}{w_*} = c_{wb}(z/z_i)^{1/3}(1 - z/z_i)^{1/3}$$

$$\frac{\sigma_{\theta b}}{\Theta_*} = c_{\theta b}\frac{(1 - z/z_i)^{2/3}}{(z/z_i)^{1/3}}$$

$$\frac{z_i}{\Theta_*}\frac{d\Theta_b}{dz} = c_{Tb}\frac{(1 - z/z_i)^{2/3}}{(z/z_i)^{4/3}}$$

$$\frac{\overline{\theta' w_b'^2}}{\Theta_* w_*^2} = c_{\theta 1b}(z/z_i)^{1/3}(1 - z/z_i)^{4/3}$$

$$\frac{\overline{\theta'^2 w_b'}}{\Theta_*^2 w_*} = c_{\theta 2b}\frac{(1 - z/z_i)^{5/3}}{(z/z_i)^{1/3}}$$

$$\frac{\overline{w'^3}}{w_*^3} = c_{3b} z/z_i(1 - z/z_1) \qquad (17)$$

and also

$$\frac{z_i dq_b}{q_* dz} = c_{Qb}\frac{(1 - z/z_i)^{2/3}}{(z/z_i)^{4/3}}$$

$$\frac{\sigma_{qb}}{q_*} = c_{qb}\frac{(1 - z/z_i)^{2/3}}{(z/z_i)^{1/3}}$$

$$\frac{\overline{\theta' q_b'}}{\Theta_* q_*} = c_{\theta qb}\frac{(1 - z/z_i)^{4/3}}{(z/z_i)^{2/3}} \qquad (18)$$

where σ is the root mean square value $c_{wb}, \ldots c_{\theta qb}$ are universal constants. Usually it is assumed that $c_{Qb} = c_{Tb}$. For small values of z/z_i, the above expressions coincide with predictions provided by the Monin–Obukhov similarity theory. Equations (17a–c) were obtained previously by Zeman and Lumley (1976) as a good fit to the experimental data within the range $0.005 < z/z_i < 0.5$.

The eddy diffusivity k_{hb} can be obtained from (15a) and (17c) by relating the temperature flux and the temperature gradient:

$$\frac{k_{hb}}{z_i w_*} = c(z/z_i)^{4/3}(1 - z/z_i)^{1/3} \qquad (19)$$

where $c = c_{tb}^{-1} = c_{Qb}^{-1}$. For small values of z/z_i, the above expression coincides with the prediction provided by the Monin–Obukhov similarity theory.

b. Tank experiments

The profiles of statistical moments (17) and (18) derived above for the case of nonpenetrative convection, can be compared with the results of tank experiments performed by Adrian et al. (1986). The authors used a tank with a 1.45 m × 1.5 m × 0.2 m test section, filled with deaerated water. The tank was heated from below by electrical mats bonded to the lower side of a smooth 2.54 cm thick aluminum plate and was heavily insulated on its top and sides. The horizontally averaged temperature was measured with a resistance thermometer. Fluctuations of temperature and horizontal and vertical velocities were measured by a thermocouple and a two-component laser Doppler velocimeter.

The obtained temperature heat flux is shown in Fig. 2. The figure indicates that the experimental profile of the heat flux is approximately a linear function of height. The profile in Fig. 2 linearly approaches a value on the surface that is approximately 20% lower than the surface heat flux. This result was not thoroughly understood by the authors and was probably caused by an accumulation of several effects introducing errors of the same sign.

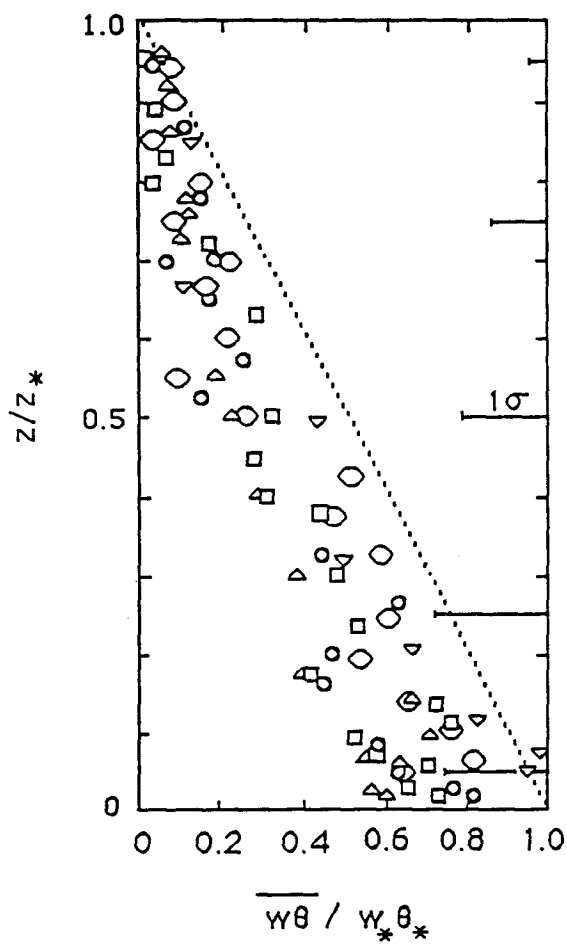

FIG. 2. Dimensionless turbulent temperature flux during tank simulation of nonpenetrative convection. Here z_* is the height of the convective layer (after Adrian et al. 1986).

The root mean square values for vertical velocity and temperature are displayed in Fig. 3. The similarity curves (17a) and (17b) were plotted for $c_{wb} = 1.05$ and $c_{\theta b} = 1.50$. The figure indicates that rising thermals decrease their temperature fluctuations as a result of heat transfers to the surrounding fluid. At the same time, their velocity increases initially, due to buoyant acceleration, and decreases in the upper part of the mixed layer as a result of heat exchange and work of compression forces. The local similarity predictions are better in the lower and middle part of the mixed layer and poorer near the upper boundary. Experimental data indicate that the root mean square temperature approaches a small and positive constant with height in the upper portion of the mixed layer. This disagrees with the similarity prediction. The similarity curve monotonically decreases to zero in the same region.

In Fig. 4, temperature flux and temperature variance transport terms are shown. The similarity curves, obtained for $c_{\theta 2b} = 1.50$ and $c_{\theta 1b} = 0.80$.

The moment $w'\theta'^2$ is large and positive near the lower boundary because thermals carry large temperature excesses in this region. It monotonically decreases with height, as shown in Fig. 4a. On the other hand, $w'^2\theta'$ initially increases with height because the vertical velocity initially increases faster with height than temperature fluctuations decrease. Above a certain level, both temperature and vertical velocity fluctuations decrease with height. As a result, $w'^2\theta'$ decreases with height in this region. Scatter in Fig. 4b appears to be larger than in Fig. 4a because values of $w'^2\theta'$ are smaller than $w'\theta'^2$.

The third moment of the vertical velocity is shown in Fig. 5. The similarity profile in the figure was plotted for $c_{3b} = 0.5$.

If the heat flux in Fig. 2 is approximated not by a linear profile (15a) but by a nonlinear one, the fit of the local similarity curves to the experimental data in Figs. 3, 4 and 5 improves. For instance, approximating the flux as $Q = Q_0[0.75 - z/z_i + 0.25(z/z_i)^2]$, causes a reduction of U_b in the upper portion of the mixed layer and a noticeable improvement in the vertical velocity statistics in this region. For the practical reason of developing a simple parameterization scheme, only formulas (17)–(18) obtained for the linear heat flux are tested in this paper.

Terms of the turbulent kinetic energy budget are shown in Fig. 6. The sum of the viscous dissipation and the pressure-energy transport were obtained as a residual in the budget equation. This sum agrees closely

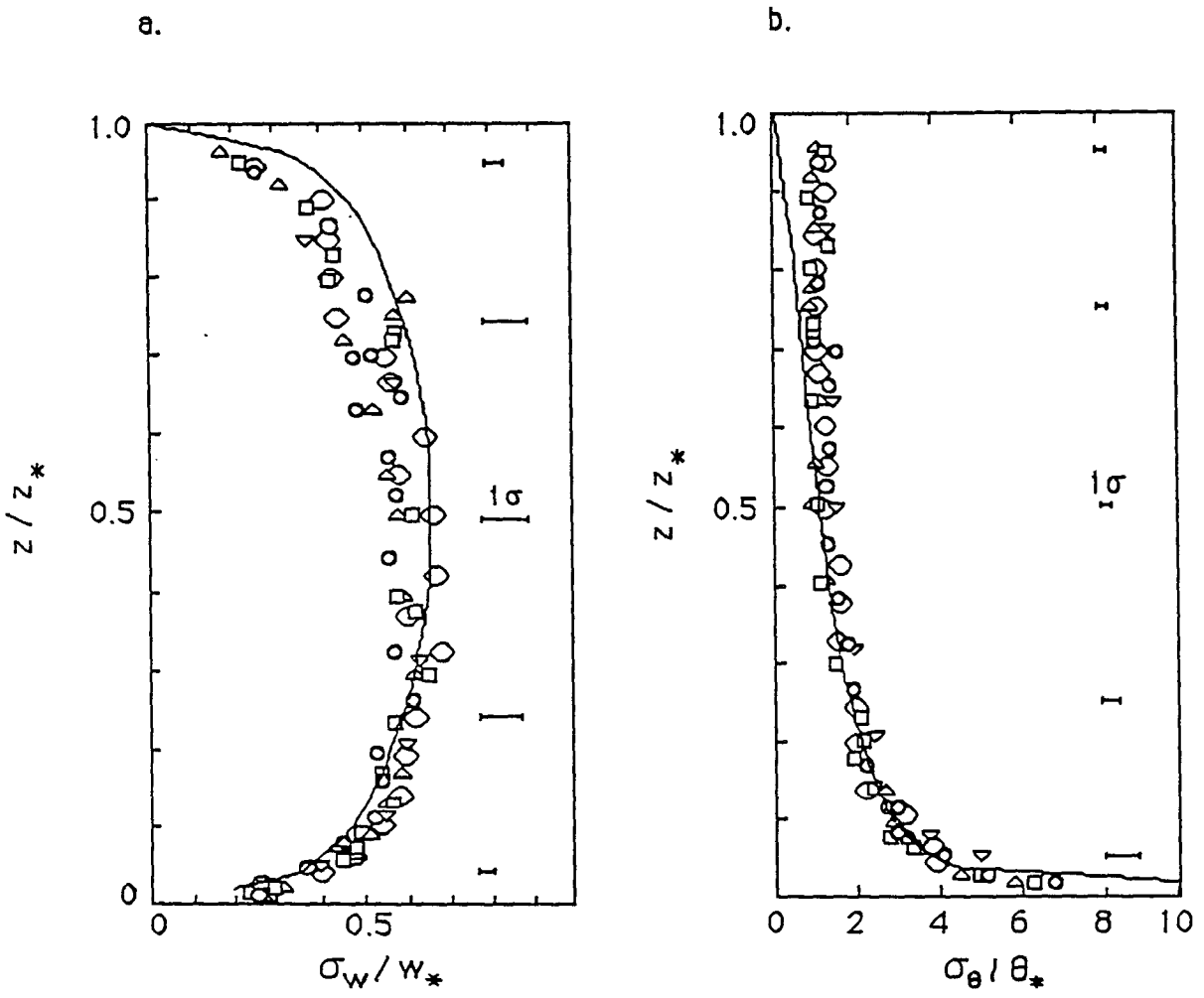

FIG. 3. Dimensionless root mean square quantities σ for (a) vertical velocity and (b) temperature, during tank simulation of nonpenetrative convection. Here z_* is the height of the convective layer. The error bars indicate the uncertainties due to statistical sampling error. (After Adrian et al. 1986.) Curves obtained from Eqs. (17a) and (17b).

with independent estimates of the dissipation rate, calculated by fitting $-5/3$ law curves to power spectra. The agreement implies that the pressure term is generally small. The vertical turbulent transport curve T in the figure was obtained from (17f) in the form:

$$\frac{1}{2}\frac{z_i}{w_*^3}\frac{d\overline{w_b'^3}}{dz} = c_{3b}(1 - 2z/z_i). \quad (20)$$

The above formula is valid above the viscous layer of the tank ($z/z_* > 0.1$), where the molecular diffusion term M can be neglected.

Equation (20) indicates that the prediction $\partial\overline{w_b'^3}/\partial z \sim U_b^3/z$, hypothesized previously by Sorbjan (1988), is incorrect. Consequently, his prediction for the dissipation rate ϵ_b is also incorrect. The dissipation rate does not follow local similarity. However, it can be evaluated from the turbulent kinetic energy budget as a difference between the buoyancy term ($=\beta\overline{w'\theta'_b}$) and the transport term ($=\frac{1}{2}\partial\overline{w_b'^3}/\partial z$):

$$\epsilon_b z_i/w_*^3 = (1 - c_{3b}/2) - (1 - c_{3b})z/z_i. \quad (21)$$

For $c_{3b} = 0.50$, one can show that the dimensionless dissipation rate changes from 0.75 near the surface to 0.25 at the top. It can be noticed that very close values of the dissipation rate were observed during atmospheric penetrative convection (e.g., Guillement et al. 1983).

Adrian et al. (1986) found that the mean temperature gradient (not shown in this paper) failed to disclose universal features described by similarity predictions. This result could be due to an inadequate separation between the tank depth z_* and the depth of the viscous sublayer z_0; i.e., an insufficiently large Reynolds number. When plotted against z/z_*, none of the empirical

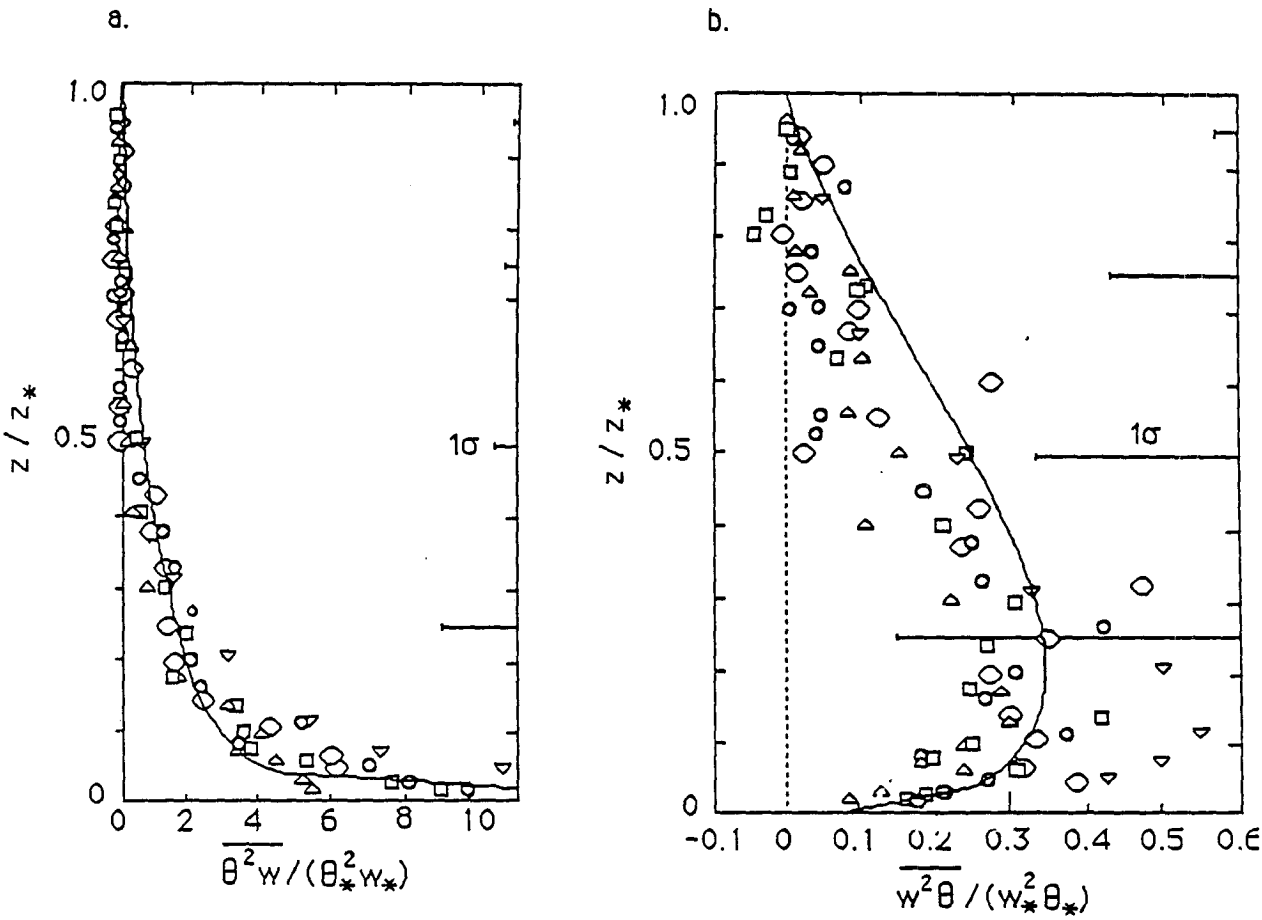

FIG. 4. Dimensionless transport terms for (a) temperature variance, and (b) turbulent heat flux, during tank simulation of nonpenetrative convection. Here z_* is the height of the convective layer. The error bars indicate the uncertainties due to statistical sampling error. (After Adrian et al. 1986.) Curve obtained from Eqs. (17d) and (17e).

curves correlated; but when plotted against $(z - 8z_0)/z_*$ they collapsed into a single curve with a slope close to the $-4/3$ in the layer up to $0.05z_*$.

LES models indicate that the mean potential temperature gradient is positive in the upper CBL during nonpenetrative convection. For instance, Moeng and Wyngaard's (1984) results show a reversal of the negative gradient for bottom-up quantities at $z/z_i \sim 0.6$, with the gradient quite positive near the top. Deardorff's (1972) tank observations in his Fig. 4 show small positive gradients in the upper portion of the mixed layer, for the two most unstable cases. These results are not reproduced by the obtained equation (17c) which yields zero values of the mean temperature gradient near the upper boundary.

Using (15), (17a) and (17b), it can be easily obtained that

$$r = \frac{\overline{w'\theta'_b}}{\sigma_{wb}\sigma_{\theta b}} = \text{const.} \qquad (22)$$

Figure 7 shows the correlation coefficient between vertical velocity and temperature. The correlation coefficient r is constant, as predicted by (22), but only in the first half of the mixed layer. Coefficient r decreases with height in the upper part of the mixed layer.

Generally, the presented model seems to give quite satisfactory results for the most of the nonpenetrative mixed layer, except near the top of the layer where its predictions are poorer.

3. Penetrative convection

Attention will now be turned to the more complex case of penetrative convection. As shown by most observational and model studies, during penetrative convection the turbulent heat and moisture fluxes are essentially linear:

$$\overline{w'\theta'}(z) = Q_0(1 - z/z_i) + Q_i z/z_i$$
$$= \overline{w'\theta'_b} + \overline{w'\theta'_t}$$

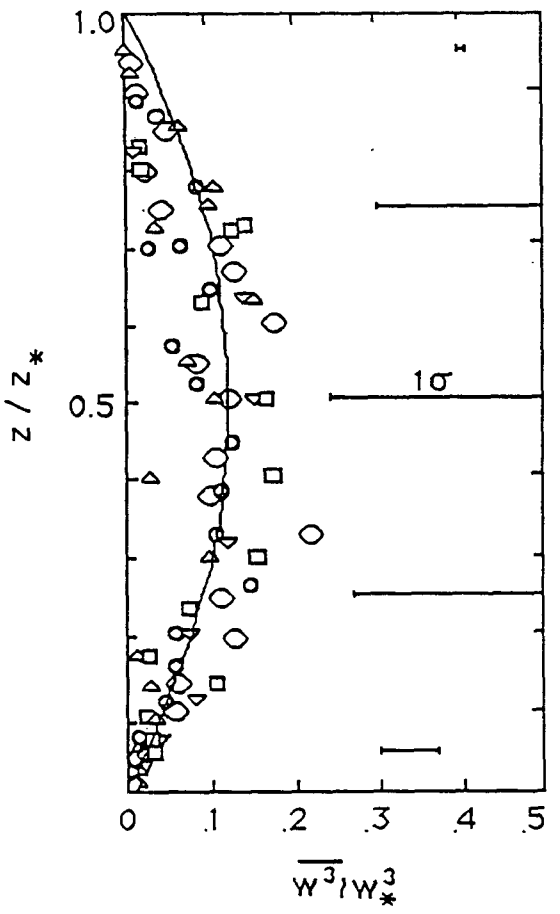

FIG. 5. Dimensionless third moment of vertical velocity during tank simulation of nonpenetrative convection, z_* is the height of the convective layer. The error bars indicate the uncertainties due to statistical sampling error. (After Adrian et al. 1986.) Curve obtained from Eq. (17f).

$$\overline{w'q'}(z) = M_0(1 - z/z_i) + M_i z/z_i = \overline{w'q'_b} + \overline{w'q'_t}, \quad (23)$$

where subscript "0" denotes the surface value and subscript "i" denotes the value at the top of the CBL. Departures from linearity are within 10% and can be ignored for simplification. An analysis of Wyngaard and Brost (1984) and Wyngaard (1984) indicates that the departure of fluxes in (23) from linear profiles can be caused by the time evolution of the mixed layer. As it follows from (9a), the consequence of linearity of the fluxes is independence of the mean temperature and humidity vertical gradients of time.

Notice that (23) is written in a form equivalent to (4). The turbulent fluxes in (23) carry the nonpenetrative terms, denoted by subscript "b," and the residual terms, denoted by subscript "t."

Further insight into the mixed layer dynamics can be gained by considering its energetics. Integration of the turbulent kinetic energy equation across the mixed layer under steady conditions and for the temperature flux distribution (23) yields (e.g., Lilly 1989):

$$\int_0^{z_i} \epsilon dz = \int_0^{z_i} \overline{w'\theta'} dz = 0.5(w_*^3 + W_*^3) \quad (24)$$

where w_* is the convective scale defined in (1) and W_* is an analogous velocity scale defined as

$$W_* = (\beta z_i Q_i)^{1/3} \quad (25)$$

The first term on the right hand side of (24) expresses production due to surface heating and the second one is consumption due to entrainment. Note that (24) has a form equivalent to (4). Since $W_* = R^{1/3} w_*$, for $R = -0.2$, it can be obtained that $W_* = -0.59 w_*$. For $(W_*/w_*)^3 = R$, from (24), it can be concluded that the portion of the energy in the mixed layer that goes into entrainment of "clear" air from above is equal to the flux ratio R, which is about 0.2. Moeng (1987) obtained the same result using conditional sampling of the results of a LES model. Equation (24) also indicates that the relative layer-averaged difference of the dissipation rates in penetrative and nonpenetrative regimes is also equal to R. This explains very close values of the dissipation rates in both regimes.

According to the parameterization (7), t-components of statistical moments are constant when scaled by the t-scales (6). The same result can be obtained in the upper part of the mixed layer for $\overline{w'\theta'}$, $\overline{w'q'}$, $\overline{\theta'q'}$, $\overline{\theta'^2}$, $\overline{q'^2}$, e^2 and $\overline{w'^2}$ from Eq. (12). Applying decomposition (4), it can be noticed that near the top of the CBL, all b-components can be neglected in these equations as being much smaller than the t-components. In addition, taking into consideration that for the "clear" air from the stable layer, all mixing lengths should be proportional to the distance from the inversion layer $Z = (z_i + \Delta - z)$, yields expressions in the form (7), as an analogy to the way the system (13) was derived. Parameterization (7) was previously examined using budget equations and proved to be valid for certain statistics of the nonpenetrative convection (Sorbjan 1989).

In the following subsections, local similarity predictions will be tested versus the LES results obtained in the case of penetrative convection by Moeng and Wyngaard (1984).

a. *Variances*

For a passive scalar (humidity) variance, Moeng and Wyngaard (1984) proposed the following decomposition:

$$\overline{q'^2} = \overline{q'^2_b} + \overline{2q'_b q'_t} + \overline{q'^2_t}. \quad (26)$$

Generally, expression (26) agrees with (4), if one treats the first term in (26) as analogous to X_b and the sum of the other two terms as analogous to X_t.

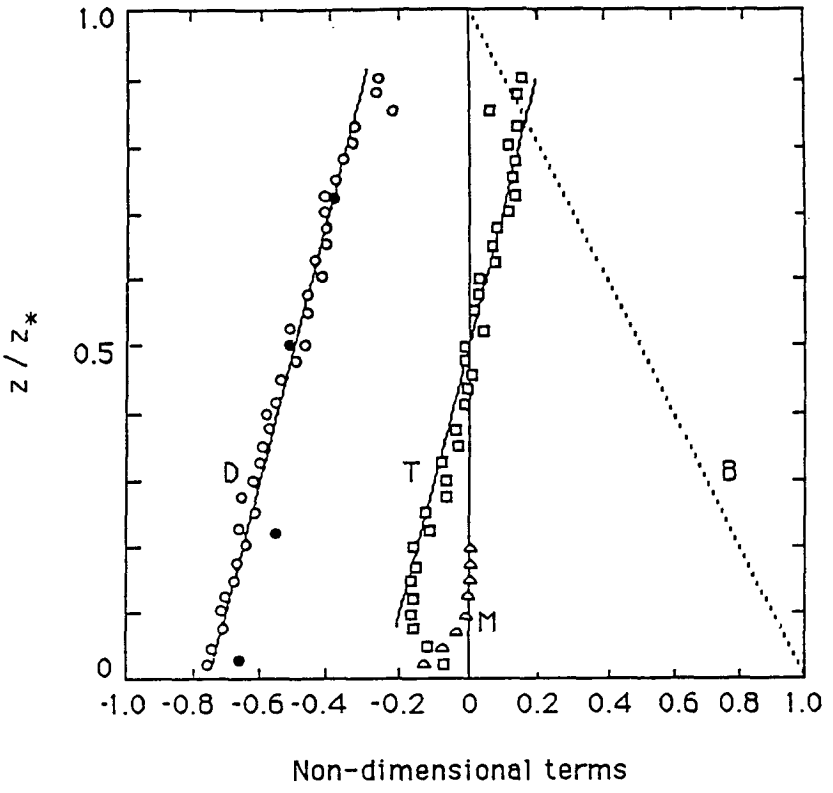

FIG. 6. Dimensionless terms in turbulent energy budget (scaled by w_*^3/z_i) during tank simulation of nonpenetrative convection: T—turbulent transport, B—buoyancy [line from Eq. (15a)], M—molecular diffusion term, D—dissipation rate plus pressure-energy transport, obtained as residuals in the turbulent kinetic energy budget (solid circles—dissipation rate evaluated by fitting $-5/3$ law curves to power spectra), z_* is the height of the convective layer (after Adrian et al. 1986).

The bottom-up (subscript b), top-down (subscript t), and mixed (subscript bt) components of the variance in (26) were expressed by Moeng and Wyngaard (1984) in terms of universal functions f_b, f_{bt}, and f_t, defined as:

$$\overline{q_b'^2} = \frac{M_0^2}{w_*^2} f_b = q_*^2 f_b$$

$$\overline{q_b' q_t'} = \frac{M_0 M_i}{w_*^2} f_{bt} = R_q q_*^2 f_{bt}$$

$$\overline{q_t'^2} = \frac{M_i^2}{w_*^2} f_t = R_q^2 q_*^2 f_t. \quad (27)$$

Moeng and Wyngaard (1984) hypothesized that for the fixed vertical velocity field (and fixed R), Eqs. (26) and (27)—derived originally for a passive scalar—can be also applied for the temperature field, which is apparently an active scalar. From this, substituting q for θ and R_q for R, it could be obtained that

$$\overline{\theta'^2} = \overline{\theta_b'^2} + \overline{2\theta_b'\theta_t'} + \overline{\theta_t'^2} \quad (28)$$

where

$$\overline{\theta_b'^2} = \Theta_*^2 f_b$$

$$\overline{\theta_b'\theta_t'} = R\Theta_*^2 f_{bt}$$

$$\overline{\theta_t'^2} = R^2\Theta_*^2 f_t. \quad (29)$$

Similarity functions f_b, f_{bt}, and f_t were evaluated from the $(40)^3$ grid-point LES model (function f_b was modified for $z/z_i < 0.3$ by using empirical data from the Minnesota experiment), and have the following form (Moeng and Wyngaard 1984):

$$f_b = 1.8(z/z_i)^{-2/3} \quad \text{for} \quad z/z_i \leq 0.1,$$
$$\text{and} \quad 0.47(z/z_i)^{-5/4} \quad \text{for} \quad z/z_i > 0.1$$
$$f_{bt} = 1$$
$$f_t = 2.1(1 - z/z_i)^{-3/2} \quad \text{for} \quad z/z_i \leq 0.9,$$
$$\text{and} \quad 14(1 - z/z_i)^{-2/3} \quad \text{for} \quad z/z_i > 0.9. \quad (30)$$

Moeng and Wyngaard (1989) found that values of the similarity functions obtained from the $(96)^3$ grid-

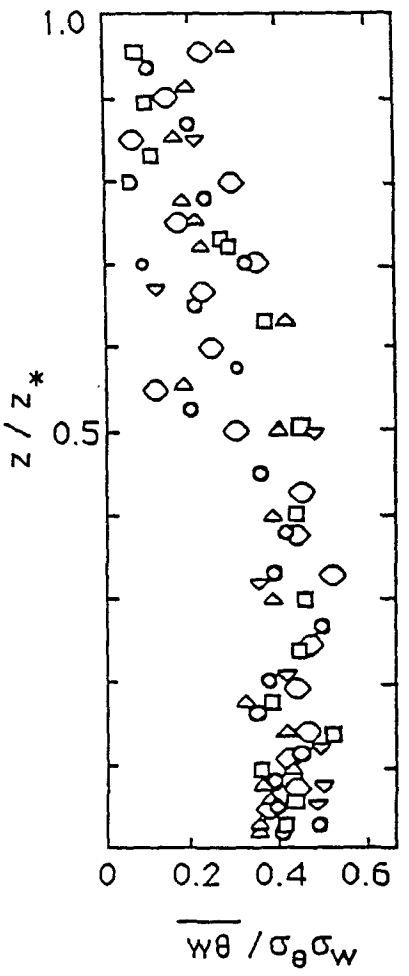

FIG. 7. Vertical velocity-temperature correlation coefficient during tank simulation of nonpenetrative convection, z_* is the height of the convective layer (after Adrian et al. 1986).

point version of the model are very close to those given by Eq. (30).

The analysis of Eq. (29) implies that "t" statistics of the temperature field in the upper part of the mixed layer change as the heat flux ratio R changes. At the same time, Eq. (27) suggests that the statistics of the passive scalar field change with the changes of the mass flux ratio R_q. On the other hand, it seems logical to expect that the humidity field should be affected by changes of the surface heat flux Q_0 [through w_* in (27)], and also by the changes of the heat flux Q_i, on the top of the mixed layer. Consequently the "bt" and "t" components of the passive scalar variance in (27) should be dependent on the heat flux ratio R.

The form of functions f in (30), obtained by Moeng and Wyngaard (1984), is valid for the particular value of $R = -0.2$, derived from the LES model. This form would be sufficient to describe the distribution of passive scalar variance in the convection boundary layer for the various values of R_q, if R was constant. However, the atmospheric and laboratory data suggest that R varies.

Tank experiments with the penetrative convection of Willis and Deardorff (1974) and Kumar and Adrian (1986) indicate that the variation of R is dependent upon the temperature lapse rate Γ in the inversion layer, above the mixed layer. The model of Zeman and Lumley (1976) shows a similar behavior and implies that R is a function of the stability-aloft parameter $S = \Gamma z_i/\Theta_*$. Here R decreases with increasing Γ. According to Willis and Deardorff (1974), this is to be expected since the penetration of fluid from the mixed region into the stable layer is confined to a smaller depth by the greater negative buoyancy of the stable layer. For small Γ, the above relation can be expected to invert (Zilitinkevich 1975). This can be explained by the fact that for decreasing Γ, the thermal contrast between the mixed layer and the layer above diminishes, consequently reducing R.

The conclusion that the passive scalar field should be affected by R can also be obtained by an analysis of the flux, variance, and covariance budgets listed in Moeng and Wyngaard's (1984) paper. The budget equations contain terms (e.g., turbulent transport and diffusion) which are clearly dependent on R in the upper part of the mixed layer.

Equation (27) is independent of R, which does not seem reasonable. Notice that using (25), one might rewrite (27) as:

$$\overline{q_b'^2} = \frac{M_0^2}{w_*^2} f_b = q_*^2 f_b$$

$$\overline{q_b' q_t'} = \frac{M_0 M_i}{w_* W_*} F_{bt} = R_q R^{-1/3} q_*^2 F_{bt}$$

$$\overline{q_t'^2} = \frac{M_i^2}{W_*^2} F_t = R_q^2 R^{-2/3} q_*^2 F_t \qquad (31)$$

where F_{bt} and F_t are new similarity functions analogous to functions f_{bt} and f_t in (27). The scale W_* allows to eliminate the dependence of the scaled quantities on R and should reduce a scatter of empirical data as a result of entrainment on the top of the mixed layer.

In analogy to the derivation of (29), for fixed R, substituting q for θ and R_q for R, it can be obtained from (31):

$$\overline{\theta_b'^2} = \Theta_*^2 f_b$$

$$\overline{\theta_b' \theta_t'} = R^{2/3} \Theta_*^2 F_{bt}$$

$$\overline{\theta_t'^2} = R^{4/3} \Theta_*^2 F_t. \qquad (32)$$

Lack of data hinders testing of the obtained expressions (31) and (32). However, their relevance can be qualitatively examined by considering the LES model. In the model, first the vertical velocity and temperature

fields are adjusted, yielding a particular value of the heat flux ratio R. After that, for fixed R, the passive scalar field and a value of R_q can be calculated. Consequently, the characteristics of the temperature field define the statistics of the passive scalar. However, since the vertical velocity field is fixed (and R is fixed), the similarity between statistics of temperature (active scalar) and the passive field is acceptable.

The relation between functions F in (31)–(32) and functions f in (27), (29) can be obtained by taking into consideration that for $R = R_0 = -0.2$ [a value obtained by Moeng and Wyngaard (1984)], (27) and (31) are equal:

$$\overline{q_t'^2} = R_q^2 q_*^2 f_t = R_q^2 R_0^{-2/3} q_*^2 F_t \qquad (33)$$

where the function f_t, in the above equation, has the form (30). Equation (33) can be rewritten as

$$F_t = R_0^{2/3} f_t = 0.342 f_t. \qquad (34)$$

Similarly, from (27) and (31), one can show that

$$F_{bt} = R_0^{1/3} f_{bt} = -0.585 f_{bt}. \qquad (35)$$

The proposed above modification of (27) and (29) implies that the formulas (31) depend on R and R_q, while the expressions (32) depend on R. For $R \to 0$ (nonpenetrative regime), the "bt"- and "t"-contributions of the temperature variance in (32) tend toward zero. Similarly, for $R_q \to 0$, the "bt"- and "t"-contributions of the variance in (31) vanish. Equations (31) has a physical sense only when R_q and R are functionally dependent in a way that they uniformly decrease, as $R \to 0$. Therefore, it is required that $R_q/R \to$ constant, for $R \to 0$. This condition is physically sound because if the heat flux on the top of the mixed layer decreases to zero, entrainment vanishes and no turbulent moisture flux should remain at this level.

Sorbjan's (1988) parameterization ignores the covariance term $\overline{\theta_b'\theta_t'}$ and has the simplified form:

$$\overline{\theta'^2} = \overline{\theta_b'^2} + \overline{\theta_t'^2} \qquad (36)$$

together with

$$\frac{\overline{\theta_b'^2}}{\Theta_*^2} = c_{\theta b} \frac{(1 - z/z_i)^{4/3}}{(z/z_i)^{2/3}}$$

$$\frac{\overline{\theta_t'^2}}{\Theta_*^2} = C_{\theta t} R^{4/3} \frac{(z/z_i)^{4/3}}{(1 - z/z_i + D)^{2/3}} \qquad (37)$$

where $C_{\theta b}$ and $C_{\theta t}$ are constants. Note that a functional dependence on R is identical in (37b) and (32c).

Figure 8 illustrates the changes of the temperature variance profile as a result of dropping the covariance, defined by (32b). The difference between two and three-term profiles of $\sigma_\theta^2/\Theta_*^2$ is equal to $-2 \times 0.585 \times R^{2/3} f_{bt} \approx -1.2R^{2/3}$ (because $f_{bt} \approx 1$) and is -0.26 for $R = -0.1$, and -0.65 for $R = -0.4$. It seems that for $R > -0.4$, the differences between two and three-term expressions are smaller than the usually observed scatter of experimental points.

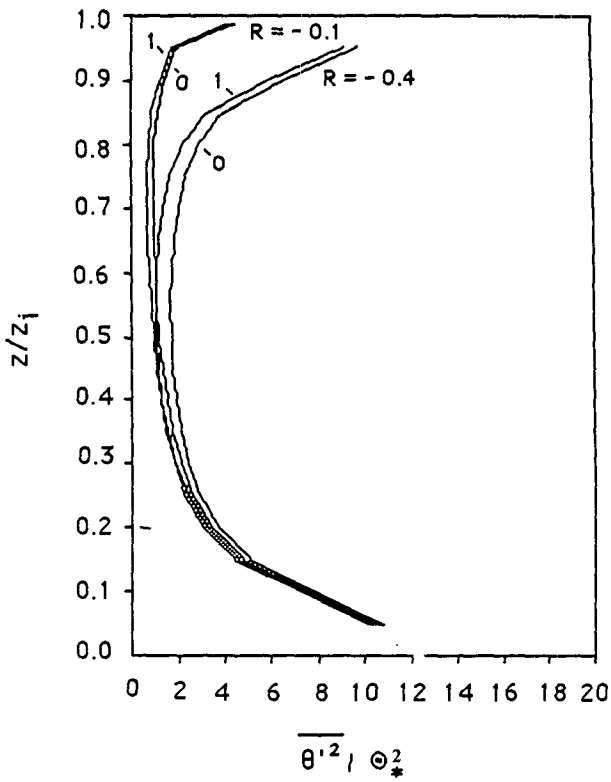

FIG. 8. Comparison of temperature variances obtained from Eqs. (28) and (32) for two values of R and for two values of covariance $\overline{\theta_b'\theta_t'}$: (0) $\overline{\theta_b'\theta_t'} = 0$, (1) $\overline{\theta_b'\theta_t'} = -0.585R^{2/3}\Theta_*^2$.

A similar figure can be obtained for the humidity variance. Because R_q is usually larger than $R(R \sim -0.1$ and $R_q \sim 1)$, the difference between the two-term and three-term curves is larger, and as it follows from (31), equal to $-2 \times 0.585 \times R_q R^{-1/3} f_{bt} \approx -1.2_q R^{-1/3}$. If ϵ is an acceptable error of σ_q^2/q_*^2 due to the dropping of the middle term, then one might require $-1.2R_q \times R^{-1/3} < \epsilon$. For $\epsilon = 1$ and $R = -0.2$, this yields $R_q < 0.49$.

Both functions $\overline{\theta_b'^2}$ and $\overline{\theta_t'^2}$, obtained from (37) for $C_{\theta b} = 2$ and $C_{\theta t} = 6$, are compared in Fig. 9 with the same functions defined by (32) using Moeng and Wyngaard's LES results (30). The figure reflects agreement of both variances. The curve shown in Fig. 3b was obtained for $c_{\theta b} = 1.5$ in (17b), which gives $C_{\theta b} = c_{\theta b}^2 = 2.25$. For comparison with Moeng and Wyngaard (1984), D was set to zero in Eq. (37). If D is assumed to be 0.1, the agreement of both functions is obtained for $C_{\theta t}$ about 1.5 times larger, $C_{\theta t} \approx 9$. Effects of parameter D are not tested in this paper due to lack of data.

It can be argued that the magnitudes of the vertical velocity and temperature fluctuations near the top of the mixed layer can be expressed by another set of

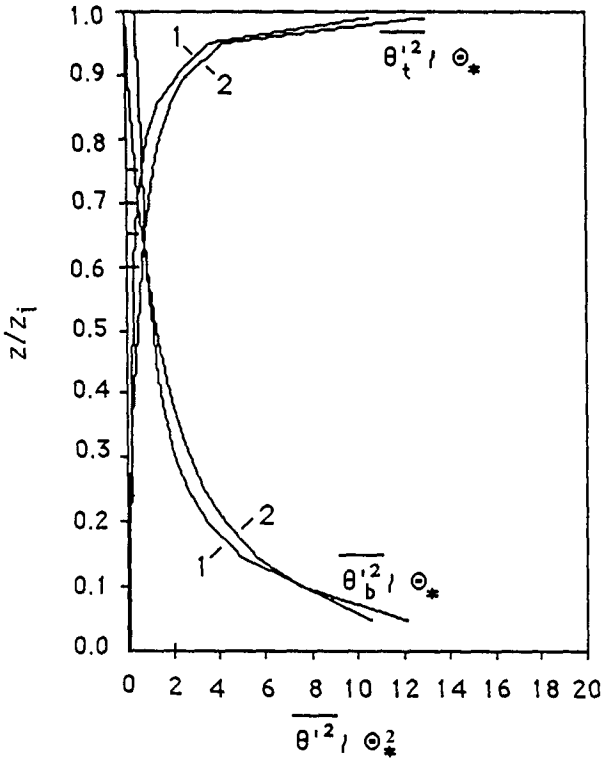

FIG. 9. Comparison of covariances $\overline{\theta_b'^2}$ and $\overline{\theta_t'^2}$ obtained from Eqs. (32) and (37), for $D = 0$ and $R = -0.2$: 1) denotes LES model results: 2) denotes similarity predictions.

scales: $w_i = (\beta \Delta Q_i)^{1/3}$, for velocity ($\Delta$ is the depth of the interfacial layer on the top of the mixed layer), and $\Theta_i = Q_i / w_i$, for temperature. Note that $w_i = w_* \times R^{1/3} D^{1/3}$ and $\Theta_i = \Theta_* D^{-1/3} R^{2/3}$. This indicates that the magnitudes of the vertical velocity and temperature fluctuations near the top of the mixed layer depend on both the surface parameters of convection w_* and Θ_*, and also on the parameters of entrainment R and D. Usually $D \sim 0.1$, $R \sim 0.2$, and consequently $w_i \sim 0.3 w_*$ and $\Theta_i \sim 0.7 \Theta_*$. Equation (37b) yields $\overline{\theta_t'^2}(z_i) = C_{\theta t} \Theta_i^2$ for $z/z_i = 1$.

b. Means

For the temperature gradient $d\Theta/dz$, Moeng and Wyngaard (1984) applied the following decomposition (similar expressions were obtained for a passive scalar gradient):

$$d\Theta/dz = d\Theta_b/dz + d\Theta_t/dz \tag{38}$$

where bottom-up (subscript b), top-down (subscript t) components of the gradient were expressed in terms of universal functions g_b and g_t, defined as

$$\frac{d\Theta_b}{dz} = -\frac{\Theta_*}{z_i} g_b$$

$$\frac{d\Theta_t}{dz} = -R \frac{\Theta_*}{z_i} g_t. \tag{39}$$

Using the analogous arguments that led to the modified expressions (31), it can be obtained for the temperature gradient:

$$\frac{d\Theta_b}{dz} = -\frac{\Theta_*}{z_i} g_b$$

$$\frac{d\Theta_t}{dz} = -R^{2/3} \frac{\Theta_*}{z_i} G_t. \tag{40}$$

In analogy to (34), there is $G_t = R_0^{1/3} g_t = -0.585 g_t$.

On the other hand, the local similarity predictions (7) yield

$$\frac{d\Theta_b}{dz} = -\frac{\Theta_*}{z_i} c_{Tb} \frac{(1 - z/z_i)^{2/3}}{(z/z_i)^{4/3}}$$

$$\frac{d\Theta_t}{dz} = -R^{2/3} \frac{\Theta_*}{z_i} c_{Tt} \frac{(z/z_i)^{2/3}}{(1 - z/z_i + D)^{4/3}}. \tag{41}$$

It can be observed that a functional dependence on R is identical in (40b) and (41b).

Equation (41) is compared with LES results in Fig. 10. Local similarity curves are plotted for $c_{Tb} = 0.6$ and $c_{Tt} = -2.0$, $R = -0.2$, $D = 0$. From (41) it follows that $d\Theta_b/dz$ is negative and decreases to zero with height. On the other hand, $d\Theta_t/dz$ is positive and increases with height from zero near lower boundary to a large value near the top of the mixed layer. The local similarity prediction that $d\Theta_b/dz \to 0$ in the upper portion of the mixed layer differs from the results of Moeng and Wyngaard (1984), who obtained positive values of the potential temperature gradient in the same region. However, in the case of the penetrative convection, near the top of the mixed layer $d\Theta_t/dz \gg d\Theta_b/dz$, and therefore this flaw of the proposed parameterization is not very serious.

It can be verified that (41) is equivalent to the k-theory flux-gradient formulation:

$$d\Theta_b/dz = -\overline{w'\theta_b'}/k_{hb}$$

$$d\Theta_t/dz = -\overline{w'\theta_t'}/k_{ht} \tag{42}$$

with two eddy diffusivities:

$$k_{hb} = U_b z / c_{Tb} = 1.7 w_* z_i (z/z_i)^{4/3} (1 - z/z_i)^{1/3}$$

$$k_{ht} = U_t Z / c_{Tt}$$

$$= 0.5 R^{1/3} w_* z_i (z/z_i)^{1/3} (1 + D - z/z_i)^{4/3}. \tag{43}$$

Wyngaard and Brost (1984) obtained from their LES model a similar result: $k_{hb} = 2.5 w_* z_i (z/z_i)^{3/2} (1 - z/z_i)$ and $k_{ht} = w_* z_i (z/z_i)(1 - z/z_i)^{3/2}$. Their eddy diffusivity k_{hb} has a maximum $[k_{hb}]_{\max} \sim 0.4$ for $z/z_i \sim 0.7$, while the local similarity expression yields $[k_{hb}]_{\max} \sim 0.7$ for $z/z_i \sim 0.8$. At the same time, Wyngaard and Brost's eddy diffusivity k_{ht} has a maximum $[k_{ht}]_{\max} \sim 0.175$ for $z/z_i \sim 0.45$, while the local sim-

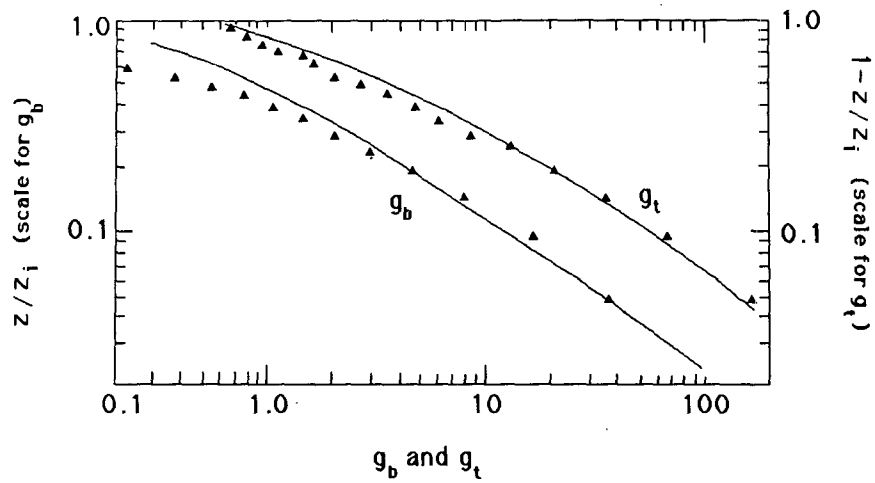

FIG. 10. The gradient functions g_b and g_t (triangles) results from LES model of Moeng and Wyngaard (1984) (lines) similarity predictions given by Eq. (41).

ilarity formulae give $[k_{ht}]_{\max} \sim 0.125$ for $z/z_i \sim 0.25$, with $R = -0.1$ and $D = 0.1$.

The eddy diffusivity evaluated as a ratio of the total (b and t components together) temperature flux and the total temperature gradient has a singularity at a certain level within the mixed layer (Sorbjan 1989). Above this level, k_h is negative and increases with height. Consequently, the local similarity parameterization is able to simulate the countergradient flux portion of the mixed layer generated by shearless, penetrative convection.

4. Summary and conclusions

The parameterization of the mixed layer, based on a decomposition of statistical moments into nonpenetrative X_b and residual X_t components and on their local (z-dependent) similarity, has been compared with the Mellor–Yamada Level-2 closure model, laboratory data, and LES results.

It has been found that the local similarity scheme for "b"-quantities, scaled by local fluxes originating from the surface and by height z, is equivalent to the Mellor–Yamada Level-2 closure model. This result was obtained assuming all length scales for nonpenetrative convection were proportional to height z. Likewise, the local similarity scheme for "t"-quantities, scaled by local fluxes originating from the base of the upper inversion and the distance Z, has been found to be equivalent to the Mellor–Yamada Level-2 closure model, at least in the upper part of the CBL. This conclusion was obtained by neglecting the (smaller) "b" components and assuming all length scales to be proportional to the distance Z from the upper inversion.

For nonpenetrative convection, assuming the heat flux drops off linearly in z, local similarity profiles for "b" components of temperature and vertical velocity moments have been shown to agree rather well with Adrian et al.'s (1986) convective tank measurements, except near the top of the mixed layer.

For nonpenetrative convection, it has been demonstrated that the local similarity decomposition is consistent with Moeng and Wyngaard's (1984) decomposition for scalar quantities. Moeng and Wyngaard's (1984) "bottom-up" and "top-down" similarity functions are equivalent to local similarity functions if the "top-down" moments are scaled by $W_* = w_* R^{1/3}$ instead of w_*. Local similarity scheme agrees fairly well with the Moeng and Wyngaard's (1984) LES results for Θ_b^2, Θ_t^2, $d\Theta_b/dz$, Θ_t/dz, except for $d\Theta_b/dz$ at $z/z_i > 0.5$.

Acknowledgments. The author would like to thank the anonymous Reviewer C for his valuable comments.

APPENDIX

List of Symbols

$D = \Delta/z_i$,	dimensionless parameter
$e^2 = \overline{u'^2} + \overline{v'^2} + \overline{w'^2}$	twice the turbulent kinetic energy
f_b, f_{bt}, f_t	similarity functions for scalar variances
F_b, F_{bt}, F_t	modified similarity functions for scalar variances
g_b, g_t	similarity functions for scalar gradients
G_b, G_t	modified similarity functions for scalar gradients
h_2	top of the interfacial layer above the mixed layer
h_1	height within the mixed layer where the heat flux is zero

k_h	eddy diffusivity
l_1, l_2, L	mixing lengths
M, M_0, M_i	moisture (passive scalar) fluxes, subscripts 0 and i indicate values of the flux at the surface and at the top of the mixed layer
$q_* = M_0/w_*$	convective humidity (passive scalar) scale
q_b, q_t	local humidity (passive scalar) scales
Q, Q_0, Q_i	potential temperature fluxes, subscripts 0 and i indicate values of the flux at the surface and at the top of the mixed layer
$R = Q_i/Q_0$	flux ratio for temperature field
$R_q = M_i/M_0$	flux ratio for humidity (passive scalar) field
R_f	flux Richardson number
$S = z_i\Gamma/\Theta_*$	stability-aloft parameter
$u_f = (\beta z Q_0)^{1/3}$	free-convection velocity scale
U_b, U_t	local velocity scales
$w_* = (\beta z_i Q_0)^{1/3}$	convective velocity scale
$w_i = (\beta \Delta Q_i)^{1/3}$	velocity scale at the top of the mixed layer
$W_* = (\beta z_i Q_i)^{1/3}$	velocity scale
z	height
z_i	height of the mixed layer
z_*	tank depth
$Z = z_i + \Delta - z$	distance from the inversion layer
$\beta = g/\Theta_0$	buoyancy parameter
ϵ	dissipation rate
Δ	depth of the interfiacial layer on the top of the mixed layer
Γ, Γ_q	temperature and humidity (passive scalar) lapse rates in the upper inversion layer
Λ_1, Λ_2	mixing lengths
σ	root mean square value
$\theta_f = Q_0/u_f$	free-convection temperature scale
Θ	potential temperature
Θ_i	temperature scale at the top of the mixed layer
Θ_b, Θ_t	local temperature scales
$\Theta_* = Q_0/w_*$	convective temperature scale

REFERENCES

Adrian, R. J., R. T. D. S. Ferreira and T. Boberg, 1986: Turbulent thermal convection in wide horizontal fluid layers. *Experiments in Fluids,* **4,** 121–141.

Deardorff, J., 1970: Convective velocity and temperature scales for the unstable planetary boundary layer. *J. Atmos. Sci.,* **27,** 1211–1213.

——, 1972: Numerical investigation of neutral and unstable planetary boundary layers. *J. Atmos. Sci.,* **29,** 91–115.

Guillement, B., H. Isaka and P. Mascart, 1983: Molecular dissipation of turbulent fluctuations in the convective mixed layer. *Bound.-Layer Meterol.,* **27,** 141–162.

Kumar, R., and R. J. Adrian, 1986: Higher order moments in the entrainment zone of penetrative thermal convection. *J. Heat Trans.,* **108,** 323–329.

Lilly, D., 1989: *Lecture Notes on Turbulence*. J. R. Herring, J. C. McWilliams, eds., Word Scientific, 171–218.

Mellor, G. L., and T. Yamada, 1974: A hierarchy of turbulence closure models for planetary boundary layers. *J. Atmos. Sci.,* **31,** 1791–1806.

Moeng, C.-H., 1987: Large-eddy simulation of a stratus-topped boundary layer. Part II: Implications for mixed layer modeling. *J. Atmos. Sci.,* **44,** 1605.

——, and J. C. Wyngaard, 1984: Statistics of scalars in the convective boundary layer. *J. Atmos. Sci.,* **41,** 3161–3169.

——, and ——, 1989: Evaluation of turbulent transport and dissipation closures in second-order modeling. *J. Atmos. Sci.,* **46,** 2311–2330.

Sorbjan, Z., 1986: On similarity in the atmospheric boundary layer. *Bound.-Layer Meteor.,* **34,** 377–397.

——, 1988: Local similarity in the convective boundary layer. *Bound.-Layer Meteor.,* **45,** 237–250.

——, 1989: Local similarity functions derived from second-moment budgets in the convective boundary layer. *Bound.-Layer Meteor.,* **465,** 1–11.

Willis, G. E., and J. W. Deardorff, 1974: A laboratory model of unstable planetary boundary layer. *J. Atmos. Sci.,* **31,** 1297–1307.

——, O. R. Coté and Y. Izumi, 1971: Local free convection, similarity, and budgets of shear and heat flux. *J. Atmos. Sci.,* **28,** 1171–1182.

Wyngaard, J. C., 1984: Toward convective boundary layer parameterization: A scalar transport module. *J. Atmos. Sci.,* **41,** 1959–1969.

——, and R. A. Brost, 1984: Top-down and bottom-up diffusion of a scalar in convective boundary layer. *J. Atmos. Sci.,* **41,** 102–112.

Yamada, T., and G. L. Mellor, 1975: A simulation of the Wangara atmospheric boundary layer data. *J. Atmos. Sci.,* **32,** 2309–2329.

Zeman, O., and J. L. Lumley, 1976: Modeling buoyancy driven mixed layers. *J. Atmos. Sci.,* **33,** 1974–1988.

Zilitinkevich, S. S., 1974: Comments on "A model for the dynamics of the inversion above a convective boundary layer." *J. Atmos. Sci.,* **32,** 991–992.